

Parameters optimization for focused ion beam fabrication of phase electron holograms

F. Venturi,^{1,2} G. C. Gazzadi²

¹Dipartimento FIM, Università di Modena e Reggio Emilia, Modena, Italy

²CNR-Istituto Nanoscienze, Modena, Italy

Corresponding author: Federico Venturi

Dipartimento FIM, Università di Modena e Reggio Emilia, Via G. Campi 213/a, I-41125 Modena, Italy

Tel. +39 059 205 5038.

E-mail: federico.venturi@unimore.it

Summary

Phase plate electron holograms allow the information of a wavefunction to be encoded onto a physical substrate (i.e. a Si₃N₄ membrane) and recovered in a transmission electron microscope in diffraction mode. One widespread means of fabrication of phase holograms is focused ion beam (FIB), however, fabrication parameters have to be carefully chosen in order to obtain the aimed results. In this work, we present the FIB fabrication of phase holograms encoding an Ince-Gaussian beam, and investigate their characteristics with varying fabrication parameters.

Key words: nanofabrication, electron holography, focused ion beam, phase holograms.

Introduzione

Since the early works of D. Gabor on electron holography (Gabor, 1948; Gabor, 1949; Gabor, 1951) and the introduction of the electron biprism (Mollenstedt and Duker, 1956), many different holographic techniques have been developed, and up to 20 different forms were counted 50 years after (Cowley, 1992). The term holography, literally “whole writing”, stands in general for those techniques that are able to encode the whole optical information of an object, i.e. its amplitude and its phase, which is then decoded by interferometric techniques (Gabor, 1956). One of the main applications of electron holography so far has been the imaging of magnetic and electric fields in matter (Pozzi, 2013), but recently also nanomanipulation (Verbeeck *et al.*, 2013) and electron beam shaping (Harris *et al.*, 2015; Grillo *et al.*, 2015) are attracting increasing interest. The particular holographic technique object of this work is that called synthetic holography (Lesem *et al.*, 1968), where the amplitude or phase information, and even both (Bolduc *et al.*, 2013; Grillo *et al.*, 2015), is encoded on a phase plate (also called kinoform (Lesem *et al.*, 1969)) and decoded when the phase plate is illuminated by a coherent source. This holographic scheme is applicable both to light optics and to electron optics, the difference lying in the kind of phase plate used:

spatial light modulators (SLMs) for light (Sampsel, 1990), transmission electron microscope (TEM) membranes for electrons (Uchida and Tonomura, 2010). While SLMs are computer-controlled and any phase profile can be easily encoded on them, TEM membranes are physical substrates that require a longer and more difficult preparation (Grillo *et al.*, 2014). Furthermore, both temporal and spatial coherence are important in order to obtain the desired interference effects; when working with a TEM, a Schottky field emission gun (FEG) is recommended, and the area occupied by the hologram should be as small as possible so that the plane wave approximation for the impinging wavefunction holds. A class of holograms that require high precision are those containing a blazed transmission grating. These holograms enhance the diffraction intensity at the first diffraction order as the blazing depth approaches a value corresponding to a 2π phase shift of the wavefront (Davis *et al.*, 1999). The phase shift of a wavefront passing through a material is linearly proportional to its mean inner potential; in this work we are using Si₃N₄ membranes, whose mean inner potential causes a 2π phase shift after a thickness of about 60 nm for 200 keV electrons (Grillo *et al.*, 2014). The aim of this paper is to investigate the influence of FIB fabrication parameters on the blazing depth, in order to approach the 2π phase shift.

Materials and Methods

Computer generation of the hologram

The wavefunctions we chose to encode on the holograms, are a class of high order Gaussian beams named Ince-Gaussian modes. They are a family of exact solutions of the paraxial wave equation described by a set of Ince polynomials, which have an intrinsic elliptical symmetry (Bandres and Gutiérrez-Vega, 2004). The generation of the hologram was done with Stem_cell software (Grillo and Rotunno, 2013), producing a bitmap pattern that was converted in an array of x and y coordinates and a value t (with $1 < t < 100$) representing the normalized greyscale intensity for each point. This so-built file is then used for FIB fabrication: x and y coordinates drive the beam position, and the t values give the beam dwell time on the point in 10^{-7} s units; the longer the dwell time the more the milling depth.

Hologram fabrication by FIB

The procedure to imprint a hologram on a membrane is composed of three steps. First, Au is deposited (~100 nm) with a sputter coater on a Si₃N₄ TEM membrane in order to inhibit electron beam transmission, then a circular area of the Au deposit is removed by FIB to let the beam pass through it, finally the previously obtained Computer Generated Hologram (CGH) is patterned on this circular area. Whereas the first two steps are quite arbitrary, the third one is the most delicate. As far as Au deposition and removal are concerned, the important thing is to obtain a thickness of the Au layer that is about 100 nm, any higher value is still good and the removal time has to be increased accordingly. The FIB cur-

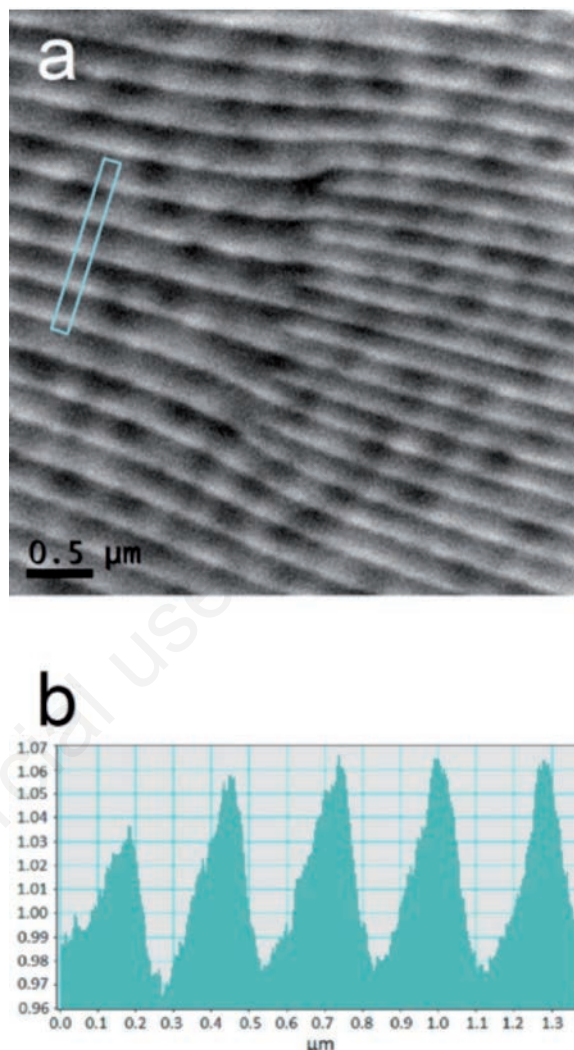


Figure 1. (a) EFTEM thickness map of the sample with starting set of parameters and (b) thickness profile calculated from the rectangular area in a.

Table 1. Sets of parameters used for samples fabrication. Notice that I2, R2, S2, M2 have the same set of parameters, which is the starting set, and are actually the same sample.

Sample	I1	I2	I3	R1	R2	R3	R4	S1	S2	S3	M1	M2	M3
Probe current (pA)	27	44	296	44	44	44	44	44	44	44	44	44	44
Repetition number	218	134	20	67	134	201	268	67	134	536	536	134	67
Step size	2	2	2	2	2	2	2	1	2	4	2	2	2
Magnification	7750X	3875X	7750X	15500X									

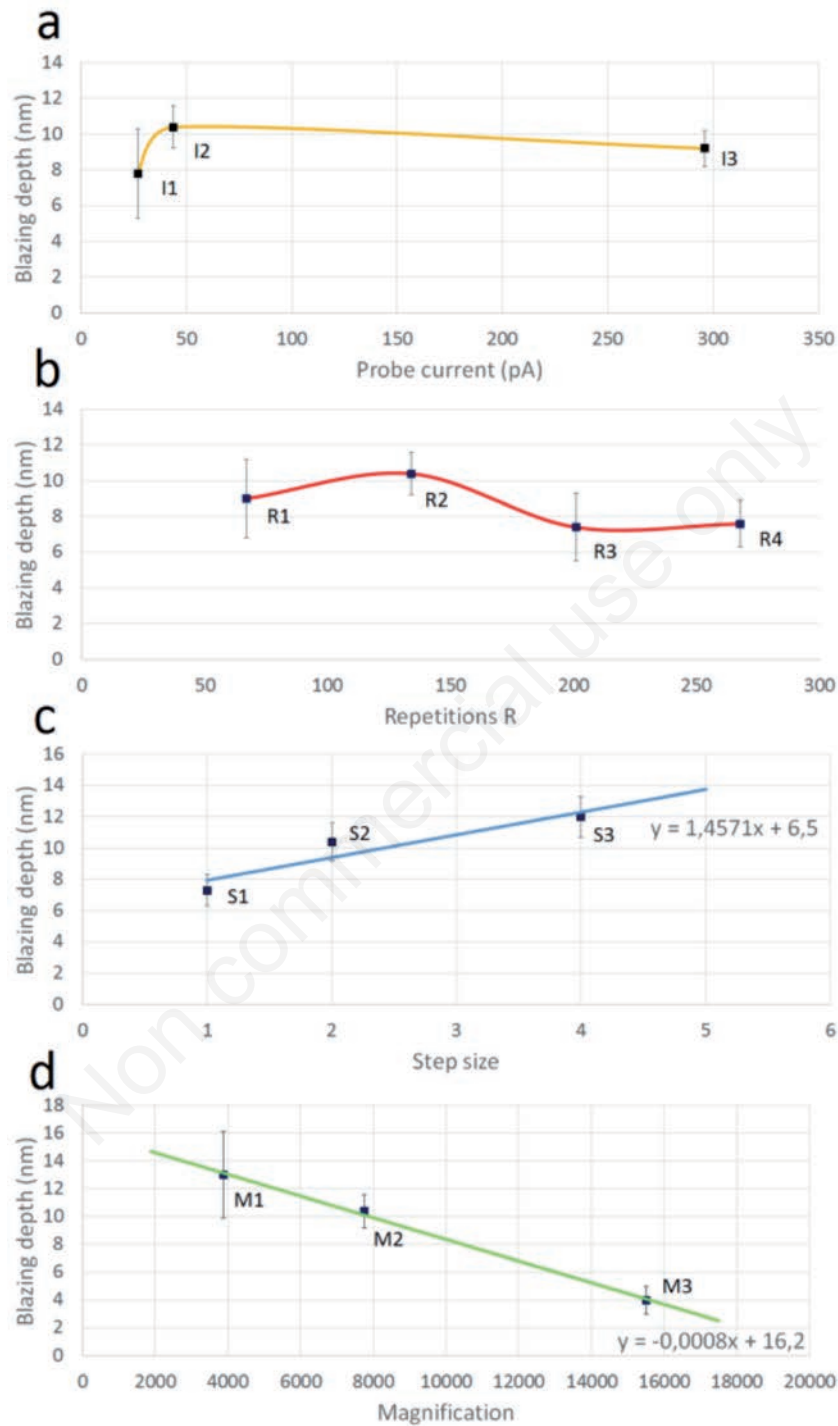


Figure 2. Trends of the blazing depth measured on samples fabricated with different varying parameters. The complete set of parameters can be found in table 1. In (a) probe current varies while step size and magnification are kept constant, in (b) repetitions vary while all the other parameters are kept constant, in (c) step size varies while probe current and magnification are kept constant, in (d) magnification varies while probe current and step size are kept constant. All the other parameters that vary are scaled in order to keep constant the number of ions per unit area. In (a) and (b) the lines are only a guide for the reader; in (c) and (d) the lines are obtained from linear fits.

rent used for Au removal can be chosen as high as needed, in order to reduce the removal time, without affecting the quality of the milling. Regarding the CGH patterning, on the contrary, many FIB parameters can have an influence on the quality of the fabrication, and these will be the object of our study.

We used a FEI Strata DB235M Dual Beam system operated at 30 kV, investigating the quality of the blazed patterning as a function of instrumental parameters like the FIB probe current (I), and on patterning parameters such as the number of repetitions (R), the step size (S) and the magnification (M). The FIB current is related to the probe size, with higher currents corresponding to larger probe sizes. The ion probe is convoluted with the hologram pattern and represents a lower boundary for the smallest feature that can be written. The number of repetitions is the

number of times the whole pattern is scanned on the substrate, it affects the overall patterning time and the maximum depth reached. The step size is the number of pixels separating two adjacent points in the patterning file; since the space of the pattern file is dimensionless, the actual dimension of the step size and of the whole pattern will depend on the magnification chosen while patterning.

TEM analyses

Once the holograms were fabricated, their analysis has been carried out inside the TEM; the microscope used is a JEOL JEM-2010 TEM operated at 200 kV, equipped with Gatan Imaging Filter (GIF). The technique used is Energy Filtered-TEM (EFTEM) thickness mapping (Williams and Carter, 2009); the thick-

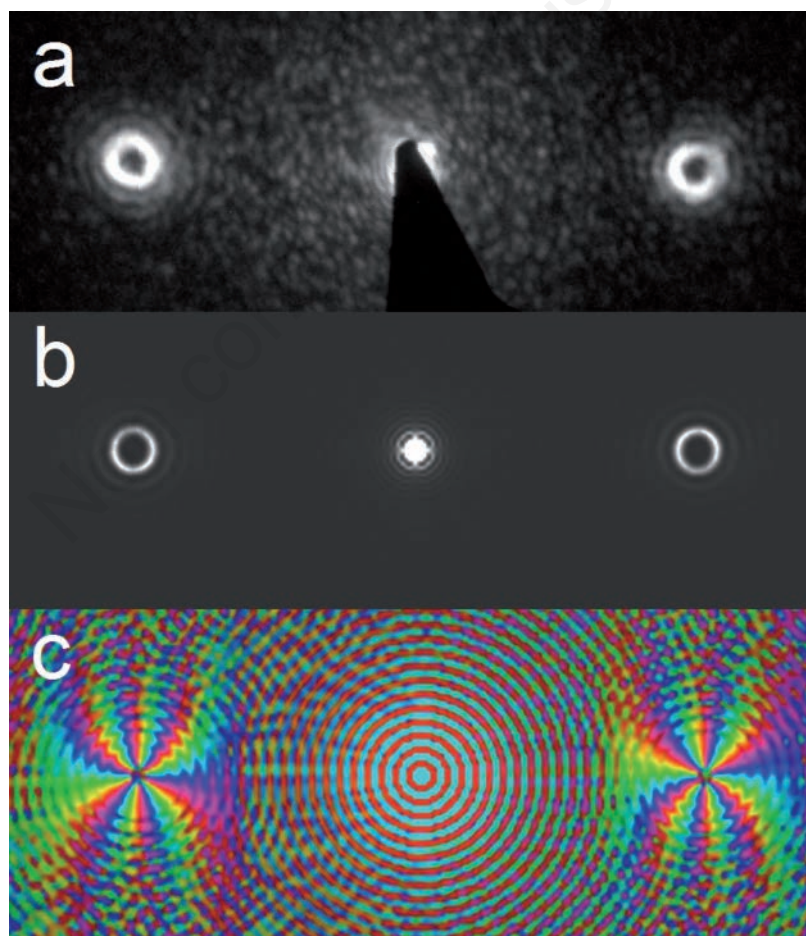


Figure 3. Diffraction pattern generated by hologram “B”: experimental intensity (a), simulated amplitude (b) and simulated phase (c). The micrograph in (a) is taken in experimental conditions where the TEM is not calibrated (high camera length), therefore any scale bar is present.

ness map data obtained with the Log-Ratio method (Egerton, 2011), expressed in number of total inelastic mean free paths (λ_i), are then converted in nanometres using the value of λ_i inside the Si_3N_4 , which is approx. 126 nm for 200 keV electrons (Egerton, 2011). From each of these maps, obtained from samples fabricated with different parameters, thickness profiles of similar zones were extracted and the average blazing depth was calculated. Furthermore, once the best fabrication parameters were determined, the hologram was observed inside a TEM in low angle diffraction mode. For this purpose, we chose a FEI Tecnai F20 ST TEM operated at 200 keV. The resulting diffraction pattern was compared with the expected amplitude and phase profiles, which were simulated with the software Stem Cell starting from the CGH.

Results and discussion

Ten holograms were fabricated with different parameters, and analysed; they belong to four different series, and each series has only one varying parameter. A *starting set* of parameters, supposed to be the best for our purposes, was chosen, and represents a jointing point of these series. This starting set of parameters is: $I = 44$ pA, $R = 134$, $S = 2$, $M = 7750X$, corresponding to an hologram area with diameter $d = 10$ μm , and minimum feature size of 280 nm. A thickness map of this sample, taken in the central zone where the dislocations are visible, is shown in fig.1a; the thicker regions appear here as brighter. The marked rectangular area is the one where the thickness profile in Fig.1b was calculated, and was chosen because it is uniform across its length, not presenting bright or dark spots, which are mainly due to the membrane surface roughness. The thickness profile in fig.1b shows the average membrane thickness, expressed in number of total inelastic mean free paths. From this profile, an average blazing depth of (10 ± 1) nm is calculated by measuring the average peak-to-valley difference and multiplying it by the mean free path length.

The same analysis was done on all the holograms; a chart with the fabrication parameters of the holograms is shown in Table 1. The results of the analyses are presented in the graphs of Figure 2. A trend of the blazing depth as a function of the FIB probe current is shown in figure 2(a): in order to conserve the overall dose, writing times (i.e. repetition number) have

been rescaled accordingly. The maximum blazing depth is reached for probe current values around 50 pA. Both higher and lower probe currents give worse results but for two different reasons: higher probe currents mean larger FIB probes with extended tails that round the features and decrease the blazing depth; lower probe currents, on the other hand, would improve spatial resolution, but the increased writing times bring in mechanical stability issues that worsen the quality of fabrication.

As far as the number of writing repetitions is concerned, we can see from Figure 2(b) that blazing depth is not proportional to the repetition number as we expected, but it has a maximum for $R=140$ and then decreases. A possible reason for this trend is the re-deposition of sputtered material in between the features, an effect that is known to limit the aspect ratio of FIB-milled nanostructures (Ishitani and Ohnishi, 1991).

Step size and magnification, instead, exhibit the expected linear behaviour, as it can be seen from the linear fit of the data in Figure 2(c) and figure 2(d). In both cases, in order to conserve the overall dose, writing times (i.e. repetition number) have been rescaled accordingly. As far as the step size is concerned, we increased the pixel interval between adjacent points of the pattern, keeping the magnification constant; as a result, the smallest patterned feature (140 nm for S1, 280 nm for S2 and 560 nm for S3) and the hologram diameter (5 μm for S1, 10 μm for S2, 20 μm for S3) were increased. As far as magnification is concerned, we kept the step size constant ($S=2$) and increased the magnification in order to obtain reversed data sets for the minimum feature size (560 nm for M1, 280 nm for M2 and 140 nm for M3) and the hologram diameter (20 μm for M1, 10 μm for M2, 5 μm for M3). Given the fact that the beam current, and so the probe size, remained constant while changing both the step size and the magnification, these results show that the limiting factor for depth resolution is the size of the beam with respect to the smallest patterned feature.

The results show that we obtain larger blazing depths with parameters corresponding to a hologram diameter of 20 μm , double than the one of the starting set of parameters. Recalling that it is fundamental to maintain high spatial and temporal coherence, a large hologram would give spatial coherence problems because the plane wave approximation for the impinging wavefunction can be valid only on a restricted area. For this reason there has to be a com-

promise between small holograms, with a high coherence condition but low blazing depth, and large holograms, with high blazing depth but low spatial coherence. In order to check if the starting set of parameters was a suitable choice, the hologram corresponding to series named I2, R2, S2 and M2, was analysed with low angle diffraction. The resulting diffraction intensity pattern is shown in figure 3(a). This pattern has to be compared with the one in figure 3(b), which is the simulated diffraction amplitude profile, obtained using the CGH. The experimental and simulated pattern agree, confirming that the chosen parameters are a suitable choice for both blazing depth and hologram area. Figure 3(c) shows then the simulated phase profile, which reveals a phase shift along one complete turn on the diffracted ring of $6 \times 2\pi$, corresponding to a beam with $6\hbar$ orbital angular momentum (OAM) (Bliokh *et al.*, 2007).

Conclusions

Electron holograms were fabricated on Si_3N_4 membranes by means of focused ion beam. Various fabrication parameters (probe current, number of repetitions, step size and magnification) were changed in

order to find the optimal conditions for a higher blazing depth. The best results were obtained for probe current of 50 pA and a number of repetitions close to 140. Increasing the step size and decreasing the magnification also led to better results due to an increase of the hologram area and to an increase of the smallest patterned feature. However, the hologram area must be kept reasonably small, in order to maintain high spatial coherence in the interferential encoding process. The sample fabricated according to the starting set of parameters was observed in low angle diffraction-TEM, and the resulting intensity profile was found to be in good agreement with the simulated amplitude profile. Phase profile was also simulated, showing that the generated beam possesses an OAM equal to $6\hbar$.

Acknowledgements

We would like to thank Stefano Frabboni from University of Modena and Reggio Emilia and Vincenzo Grillo from CNR-Nano S3 Modena for their kind support. Part of the experimental work done by Roberto Balboni at CNR-IMM Bologna is gratefully acknowledged.

References

- Bandres MA, Gutiérrez-Vega JC. Ince-Gaussian beams. *Optics Letters* 2004;29(2):144-6.
- Bliokh KY, Bliokh YP, Savel'ev S, Nori F. Semiclassical dynamics of electron wave packet states with phase vortices. *Phys. Rev. Lett.* 2007;99:190404.
- Bolduc E, Bent N, Santamato E, Karimi E, Boyd RW. Exact solution to simultaneous intensity and phase encryption with a single phase-only hologram. *Optics Letters* 2013;38(18):3546-9.
- Cowley JM. Twenty forms of electron holography. *Ultramicroscopy* 1992;41:335-48.
- Davis JA, Cottrell DM, Campos J, Yzuel MJ, Moreno I. Encoding amplitude information onto phase-only filters. *Appl. Optics* 1999;38(23):5004-13.
- Egerton RF. *Electron Energy-Loss Spectroscopy in the electron microscope*. 3rd ed. New York: Springer; 2011.
- Gabor D. A new microscopic principle. *Nature* 1948;161:777-8.
- Gabor D. Microscopy by reconstructed wave-fronts. *Proc. Roy. Soc. A* 1949;197:475.
- Gabor D. Microscopy by reconstructed wave fronts: II. *Proc. Phys. Soc. B* 1951;64:244.
- Gabor D. Theory of electron interference experiments. *Rev. Mod. Phys.* 1956;28(3):260.
- Grillo V, Rotunno E. STEM_CELL: A software tool for electron microscopy: part I - simulations. *Ultramicroscopy* 2013;125:97-111.
- Grillo V, Gazzadi GC, Karimi E, Mafakheri E, Boyd RW, Frabboni S. Highly efficient electron vortex beams generated by nanofabricated phase holograms. *Appl. Phys. Lett.* 2014;104:043109.
- Grillo V, Pierce JS, Karimi E, Harvey TR, Balboni R, Gazzadi GC, et al. Structured electron beam illumination: a new control over the electron probe weird probes and new experiments. *Microsc. Microanal.* 2015;21(S3):25.
- Grillo V, Karimi E, Balboni R, Gazzadi GC, Venturi F, Frabboni S, et al. Electron holograms encoding amplitude and phase for the generation of arbitrary wavefunctions. *Microsc. Microanal.* 2015;21(S3):503.
- Harris J, Grillo V, Mafakheri E, Gazzadi GC, Frabboni S,

- Boyd RW, et al. Structured quantum waves. *Nature Physics* 2015;11(8):629-34.
- Ishitani T, Ohnishi T. Modeling of sputtering and redeposition in focused-ion-beam trench milling. *J. of Vacuum Science & Technology A* 1991;9:3084.
- Lesem LB, Hirsch PM, Jordan JA. Computer synthesis of holograms for 3-D display. *Jr. Commun. (ACM)* 1968;11:661-74.
- Lesem LB, Hirsch PM, Jordan JA. The kinoform: a new wavefront reconstruction device. *IBM Jr. of Research and Development* 1969;13:150-5.
- Mollenstedt G, Duker H. Beobachtungen und messungen an biprisma-interferenzen mit elektronenwellen. *Z. Phys.* 1956;145:377-9. German.
- Pozzi G. *Microscopia e olografia con elettroni*. 1st ed. Bologna: Bononia University Press; 2013. Italian.
- Sampsel JB, inventor; Texas instruments Inc., assignee. Spatial light modulator. United States patent US 4954789. 1990 Sep 4.
- Uchida M, Tonomura A. Generation of electron beams carrying orbital angular momentum. *Nature* 2010;464:737-9.
- Verbeeck J, Tian H, Van Tendeloo G. How to manipulate nanoparticles with an electron beam?. *Advanced Materials* 2013;22(8):1114-7.
- Williams DB, Carter CB. *Transmission electron Microscopy*. 2nd ed. New York: Springer; 2009.

Non commercial use only